

Neural networks as a tool for parameter estimation in astrophysical data

Nicholas G. Phillips ¹

*SSAI, Laboratory for Astronomy and Solar Physics, Code 685, NASA/GSFC, Greenbelt,
Maryland 20771*

and

Alan J. Kogut ²

*Laboratory for Astronomy and Solar Physics, Code 685, NASA/GSFC, Greenbelt, Maryland
20771*

October 25, 2018

ABSTRACT

We present a neural net algorithm for parameter estimation in the context of large cosmological data sets. Cosmological data sets present a particular challenge to pattern-recognition algorithms since the input patterns (galaxy redshift surveys, maps of cosmic microwave background anisotropy) are not fixed templates overlaid with random noise, but rather are random realizations whose information content lies in the correlations between data points. We train a “committee” of neural nets to distinguish between Monte Carlo simulations at fixed parameter values. Sampling the trained networks using additional Monte Carlo simulations generated at intermediate parameter values allows accurate interpolation to parameter values for which the networks were never trained. The Monte Carlo samples automatically provide the probability distributions and truth tables required for either a frequentist or Bayesian analysis of the one observable sky. We demonstrate that neural networks provide unbiased parameter estimation with comparable precision as maximum-likelihood algorithms but significant computational savings. In the context of CMB anisotropies, the computational cost for parameter estimation via neural networks scales as $N^{3/2}$. The results are insensitive to the noise levels and sampling schemes typical of large cosmological data sets and provide a desirable tool for the new generation of large, complex data sets.

¹email: Nicholas.G.Phillips.1@gsfc.nasa.gov

²emai: Alan.J.Kogut.1@gsfc.nasa.gov

1. Introduction

A fundamental question in cosmology is the origin and evolution of large scale structure in the universe. The standard model for this evolution is the gravitational growth and collapse of initially small perturbations in the primordial density distribution. This picture is supported by the detection of primordial Cosmic Microwave Background (CMB) temperature anisotropies at a level of approximately one part in 10^5 by the Cosmic Background Explorer (COBE) satellite and a series of ground-based and balloon-borne experiments. Small perturbations on the matter and energy density in the early universe are reflected in the temperature distribution of the CMB, providing a “snapshot” of conditions the early universe while the perturbations were still in the linear regime.

One angular scale of particular interest is the horizon size at the surface of last scattering, the epoch when the universe cooled sufficiently to form neutral hydrogen and allow the CMB photons to propagate freely. Causally-connected regions at the surface of last scattering, as viewed from the present epoch, subtend an angle

$$\theta \sim 1.7^\circ \Omega_0^{1/2} \left(\frac{1100}{1 + z_{ls}} \right)^{1/2}$$

where z_{ls} is the redshift at last scattering and Ω_0 is the total density of the universe relative to the critical (closure) density. Anisotropy on scales larger than $\sim 2^\circ$ reflect perturbations larger than the particle horizon and thus probe the primordial density distribution. On scales smaller than 2° , causal mechanisms become important and modify the primordial density in model-specific ways.

From the one observable sky, we want to infer the values of these cosmological parameters with minimal uncertainty in the shortest possible time. Theoretical models do not predict a specific template for the CMB anisotropy (a hot spot at this location, a cold spot over there), but rather predict a statistical distribution usually expressed in terms of the angular power spectrum. Deriving the power spectrum from the data (or more generally, deriving model parameters directly from the sky maps) involves accounting for angular correlations between pixels, precluding use of simple linear least-squares techniques. The accepted standard in the CMB community has been the generalization of least-squares techniques as implemented in maximum likelihood algorithms (see, e.g., Górski et al. 1996; Tegmark, Taylor, & Heavens 1997; Bond, Jaffe, & Knox 1998; Borrill 1999).

The simplest method of parameter estimation uses a goodness-of-fit test to compare a set of observables $y_i \pm \sigma_i$ measured at a set of positions x_i to a theoretical model Γ_i . If we have N_d data points y_i and N_p parameters p_j , we define

$$\chi^2 = \sum_{i=1}^{N_d} \left(\frac{y_i - \Gamma_i}{\sigma_i} \right)^2, \quad (1)$$

where

$$\Gamma_i(x) = \sum_{j=1}^{N_p} p_j X_j(x_i) \quad (2)$$

is function of the parameters p and some fixed basis functions $X(x)$. We obtain the “best-fit” parameter values by minimizing χ^2 with respect to the parameters,

$$\frac{\partial \chi^2}{\partial p_j} = 0 \quad (3)$$

for the j^{th} parameter p_j . The least-squares system in Eq. 3 has the solution

$$p_j = \sum_{k=1}^{N_p} (\mathbf{A}^{-1})_{jk} B_k \quad (4)$$

where

$$\mathbf{A}_{jk} = \sum_{i=1}^{N_d} \frac{X_j(x_i) X_k(x_i)}{\sigma_i^2} \quad (5)$$

is an $N_p \times N_p$ matrix, and

$$B_k = \sum_{i=1}^{N_d} \frac{y_i X_k(x_i)}{\sigma_i^2} \quad (6)$$

is a vector of length N_p .

If the data points are not independent, this relatively simple calculation becomes much more costly. Covariance between the observed data points can result from instrumental artifacts (correlated noise, instrumental resolution, oversampled data) or from correlations in the underlying signal (for instance, measuring in real space a signal whose components are independent in Fourier space). Equation 1 can be generalized to include the effects of covariance,

$$\chi^2 = \sum_{i=1}^{N_d} \sum_{j=1}^{N_d} (y_i - \Gamma_i) (\mathbf{M}^{-1})_{ij} (y_j - \Gamma_j), \quad (7)$$

where

$$\mathbf{M}_{ij} = \langle (y_i - \langle \Gamma_i \rangle) (y_j - \langle \Gamma_j \rangle) \rangle \quad (8)$$

is the $N_d \times N_d$ covariance matrix and the brackets denote an ensemble average.

Conjugate gradient techniques can solve for χ^2 without expliciting solving for \mathbf{M}^{-1} and thus avoiding the $O(N_d^3)$ operations this would incur. But if the covariance matrix \mathbf{M} depends on the parameters p_j , then minimizing χ^2 will produce biased estimates for p_j . Maximum-likelihood parameter estimation provide a tool to overcome this limitation. For a multivariate Gaussian distribution, the probability of obtaining the observed data y_i given a set of parameters p_j is

$$\mathcal{L} = P(y|p) = (2\pi)^{-N_d/2} \frac{\exp(-\frac{1}{2}\chi^2)}{|\mathbf{M}|^{1/2}} \quad (9)$$

where χ^2 is defined in Eq. 7. The “best” choice of parameters is that which maximizes the likelihood function \mathcal{L} . The curvature of the likelihood surface about the maximum defines the uncertainty in the fitted parameters,

$$\delta p_j \geq \sqrt{(\mathbf{F}^{-1})_{jj}} \quad (10)$$

where

$$\mathbf{F}_{ij} = \left\langle \frac{\partial^2 L}{\partial p_i \partial p_j} \right\rangle \quad (11)$$

is the Fisher information matrix (Kendall & Stuart 1969) and $L = -\log(\mathcal{L})$ (see Bunn & Sugiyama 1995; Vogeley & Szalay 1996; Tegmark et al. 1997; Bond et al. 1998).

The maximum likelihood estimator is unbiased and asymptotically approaches the equality in Eqn. 10. However, these advantages come at a steep price: both the χ^2 and the determinant calculation in Eq. 9 scale as $O(N_d^3)$, making brute-force techniques computationally infeasible. For $N_d > 10^6$ the time required is measured in years, even on the most powerful supercomputers. A number of authors have suggested ways around this limitation, see *e.g.* Oh Spergel & Hinshaw 1999, Hivon, *et. al.* 2001 and Doré, Knox & Peel 2001. Such methods usually rely on symmetries in the data, *i.e.*, axial symmetry of the noise, while neural networks need to make no assumptions about symmetries.

Neural networks provide an alternative for astrophysical parameter estimation. They have been used previously in astronomy for galaxy classification (Lahav *et. al.* 1996; Andreon *et. al.* 2000) and periodicity analysis of unevenly sampled data as applied to stellar light curves (Tagliaferri *et. al.* 1999). They have also been used to analyze stellar spectra (Bailer-Jones *et. al.* 1997; Bailer-Jones *et. al.* 1998; Bailer-Jones 2000), with results comparable to traditional methods. However, Bailer-Jones *et. al.* compared data to a deterministic model (stellar spectra), whereas cosmological applications examine random patterns drawn from parameterized stochastic models. We demonstrate the generality of our algorithm by considering different problems with the same network architecture. We find the computational cost for training the network, in the context of CMB anisotropy, requires $O(N^{3/2})$ operations and thus provides a substantial improvement over brute-force maximum-likelihood methods.

The stochastic nature of our models is fundamental: their starting point is the quantum nature of the early universe. What the models predict are the parent populations from which individual realizations are to be drawn. Our single observed universe is assumed to be such a realization. The question becomes: given a particular model, which parameters that define the parent population best describe the observed data? This is to be contrasted with the problems of stellar spectra or galaxy classification, which have at their heart either a deterministic model or a pre-assigned catalogue of types.

This stochastic nature means any analysis of the observed data must rely on some statistical test. Leaving aside for the moment the computational challenges of traditional maximum likelihood methods, this raises the problem of knowing the best statistic for distinguishing between different parameters or models (we can view model selection as a discrete parameter to be estimated). Maximum likelihood methods require an *a priori* definition of a goodness-of-fit function. The choice of a goodness-of-fit function is not always obvious and is particularly acute for 2D and 3D surveys. Much of the information lies in the *phase* features of these surveys. Statistical tests can fail badly in detecting phase features, as witness the large literature devoted to

the relatively simple problem of edge detection in 2D data sets (see, e.g., Hough 1962 and Davis 1975). Topological tests such as the genus or other Minkowski functionals have been applied to 2- and 3-D maps, (Gott *et. al.* 1990; Kogut *et. al.* 1996) but the relative power of these statistics is poor (Phillips & Kogut 2001). Neural networks, in contrast, do not require specification of a single statistic of *a priori* interest. As the network is trained, it determines how it will discriminate between competing models.

All observations add instrumental effects to the desired physical signal. Any analysis of the data must model these effects. For neural networks, this presents no great challenge as long as we can model the effects. For either irregularly sampled time series data or 2D/3D survey data with missing patches, any analysis based on Fourier methods will suffer from aliasing of power. With neural networks, this problem does not arise; by excluding from the simulations the data points missing in the observed data, the networks will learn the effects of the gaps. The inclusion of noise to the simulations may increase the number of training passes needed, but will not prevent the use of neural networks for parameter estimation.

2. Neural Network

Neural networks can be trained to estimate the value of a continuous parameter, and can reliably interpolate to parameter values intermediate between the training values. Though this idea is not new to astrophysics, *e.g.* (Bailer-Jones *et. al.* 1997; Bailer-Jones *et. al.* 1998; Bailer-Jones 2000), our method is fundamentally different from that of Bailer-Jones *et. al.* in that our patterns are random samples drawn from a parameterized parent population. The Bailer-Jones *et. al.* method is a matter of template matching; randomness only enters their input patterns as instrument noise. For CMB and other cosmological data, the patterns themselves are intrinsically random. Nonetheless, using the same basic neural network architecture, we can train the networks to discriminate stochastic patterns that differ according to the parent population from which they are drawn.

We start by training a network to differentiate between simulated data sets (including instrument noise and other artifacts) generated at a pair of discrete parameter values. The back-propagation adjusts the weights until the network outputs target value 0 when presented with the first set of patterns, and target value 1 when presented with the second. In practice, since the information distinguishing different parameter values is in the correlations, not the actual pixel values, any single network will not train to a sufficient degree. We improve the situation by training a small committee of networks and polling them to get a consensus opinion. Now we find simulations generated at the training parameter values produce two well defined peaks. Simulations generated with an intermediate parameter value (never present in training data) yield outputs peaking somewhere in between, depending on whether the new parameter value is closer to the first or second training value (see Fig 2).

We quantify this behavior by presenting the trained network with a set of new inputs drawn

from a grid of intermediate parameter values, and derive for each intermediate parameter value the corresponding probability distribution of output values. When the networks are later presented with an unknown pattern, each distribution gives the probability that the unknown pattern was generated with a parameter value corresponding to that grid point. The interpolated parameter is the probability-weighted mean. The grid samples all use the same trained networks; the sampling of the networks at different grid points is faster than the training since we usually need many more training sets than sampling sets, thus no great computational cost is incurred. This sort of sampling of trained networks becomes a key component in utilizing a Bayesian approach to parameter estimation, see Christensen and Meyer 2000 and Rocha *et. al.* 2000 for discussions of the Bayesian approach in the context CMB anisotropies and MacKay 1995, along with Bishop 1995 for neural networks. Although we focus below on estimating a single parameter, the method is readily extended to multi-parameter fits.

2.1. Parameter estimation via the Bayesian approach

We use the standard MLP: $y_k^l = f(\sum_{i=0}^{N_{l-1}} w_{ki}^l y_i^{l-1})$, where y_k^l is the output of neuron k for layer l , N_l is the number of neurons in layer l and w_{ki}^l is the weight connecting neuron i of layer $l - 1$ with neuron k of layer l . We include a bias for each neuron via $y_0^l = 1$. The activation function is the sigmoid $f(x) = 1/(1 + e^{-x})$. We only consider networks with the fully-connected, single hidden layer topology and a single output neuron. The number of weights per network is $N_{\text{wgt}} = N_{\text{hidden}}(N_{\text{input}} + 2) + 1$.

We use standard backpropagation for training, with weight updates after each training point. The quadratic cost function is used: $E = \frac{1}{2}(o_{\text{patt}} - t_{\text{patt}})^2$, where $o_{\text{patt}} = y^{\text{output layer}}(\mathbf{X}_{\text{patt}})$ is the network output when presented with the input \mathbf{X}_{patt} and t_{patt} is the desired target for that pattern.

The input patterns \mathbf{X} are the end product of our simulations and as such are realizations taken from an underlying parameterized probability distribution with parameter p . Thus we label each input pattern by the parameter from which it was drawn: $\mathbf{X}(p)$. Assuming the data lies between two extreme values $p^{(0)}$ and $p^{(1)}$ we train a network to the target $t^{(0)} = 0$ for realizations $\mathbf{X}(p^{(0)})$ and $t^{(1)} = 1$ for $\mathbf{X}(p^{(1)})$ by repeatedly presenting the network with new samples at $p^{(0)}$ and $p^{(1)}$ and back propagating the error. Once trained, the network will give an output $o(\mathbf{X})$ between 0 and 1 for any input parameter value. If $p < p^{(0)}$, the output clips at 0, while if $p > p^{(1)}$ the output clips at 1.

Once we have trained a network, we can present additional, statistically independent samples drawn at $p^{(0)}$ and $p^{(1)}$. Figure 2a shows the output distributions for 1000 patterns of each parameter. We see the network has successfully trained in that the $p^{(0)}$ distribution is peaked at $o = 0$ while the $p^{(1)}$ samples at $o = 1$. To be able to interpolate to intermediate values, we will need to present samples drawn at intermediate parameter values. Fig 2b shows the output distributions for an additional 1000 samples each for two parameters, one just a little larger than $p^{(0)}$ and one a little

smaller than $p^{(1)}$. These distribution also show the same tendency to peak close to the limits of 0 and 1, but not as strongly as those drawn at the trained parameters. In effect, the network is choosing which of the training parameters these new patterns, for which it was never trained, most closely resemble. At it stands now, this tendency makes it hard to construct the probability distributions we need for parameter estimation.

By using a committee of networks, we take advantage of this peaking tendency. We want to determine the committee consensus and from this get the distributions we seek. The first step is converting the continuous output value into a discrete *truth values* 0 or 1. For each trained network, we associate a midpoint value o_{mid} and for any input pattern \mathbf{X} , we define its truth value according to

$$\mathbf{t} \equiv \mathbf{t}(\mathbf{X}) = \begin{cases} 0; & o(\mathbf{X}) \leq o_{\text{mid}} \\ 1; & o(\mathbf{X}) > o_{\text{mid}} \end{cases} . \quad (12)$$

We interpret $\mathbf{t}(\mathbf{X}) = 0$ as indicating the pattern was drawn from the parent population with parameter $p^{(0)}$, and similarly we associate $\mathbf{t} = 1$ with $p^{(1)}$.

To determine o_{mid} , we present N samples drawn at $p^{(0)}$ and N samples at $p^{(1)}$. For each of these sets and any \tilde{o}_{mid} , we obtain the truth values $\mathbf{t}_i^{(0)}$ and $\mathbf{t}_i^{(1)}$, $i = 1, \dots, N$. With this, $\mathbf{n}^{(0)} = \sum_i (1 - \mathbf{t}_i^{(0)})$ is the number patterns drawn at $p^{(0)}$ correctly identified as drawn at $p^{(0)}$ and $\mathbf{n}^{(1)} = \sum_i \mathbf{t}_i^{(1)}$ similarly at $p^{(1)}$. We chose o_{mid} to maximize $f_C = \frac{1}{2N}(\mathbf{n}^{(0)} + \mathbf{n}^{(1)})$ and refer to f_C as the *fraction correct*, our main measure of how well a network has trained. In Fig 2a, o_{mid} is marked with the vertical line and we find $f_C = 94\%$.

We note f_C allows us to determine the optimal number of training passes, N_{Train} . Starting with an initially randomized network, as the network trains, we intermittently pause the training and sample the network to determine f_C . It steadily increases to a maximum value and then levels out: the minimum for the training error E has been reached. We take N_{Train} to be just where this plateau starts and thus avoid overtraining.

For each network, any given input pattern is converted into discrete truth values \mathbf{t} . We now form a committee of such networks, where the only difference between the networks is the initial randomization of the weights. We find committee sizes $N_{\text{net}} \sim 50$ sufficient. After presenting any given pattern \mathbf{X} to the committee, we have the collection of truth values $\mathbf{t}(\mathbf{X})_m$, $m = 1, \dots, N_{\text{net}}$. We view each \mathbf{t}_m as the vote from network m as to whether the pattern resembled those drawn at $p^{(0)}$ or $p^{(1)}$. The committee consensus is formed by generating the *average truth value*

$$\bar{\mathbf{t}}(\mathbf{X}) = \frac{1}{N_{\text{net}}} \sum_{m=1}^{N_{\text{net}}} \mathbf{t}(\mathbf{X})_m . \quad (13)$$

Figure 2c shows the distribution of average truth values for the same set of samples drawn at $p^{(0)}$ and $p^{(1)}$ used in Fig 2a. They are now even more sharply peaked about $\bar{\mathbf{t}} = 0$ and $\bar{\mathbf{t}} = 1$ and in terms of the average truth value, $f_C = 100\%$. More important are the distributions displayed in Fig 2d. These are for the same intermediate samples as used in Fig 2b; we have now two well

defined distributions with peaks intermediate to the peaks for the $p^{(0)}$ and $p^{(1)}$ samples. This is the general trend when we work in terms of the average truth value: as the parameter p is swept from $p^{(0)}$ to $p^{(1)}$, we get well defined distributions whose peak moves from $\bar{\tau} \sim 0$ to $\bar{\tau} \sim 1$.

When we present our committee with an observed pattern, \mathbf{X}_{obs} , for which we do not know the parameter, we get its average truth value $\bar{\tau}_{\text{obs}}$. From the Bayesian viewpoint, we are interested in the posterior distribution $\mathcal{P}(p|\bar{\tau}_{\text{obs}})$: given the observation, what is the probability the true parameter is p . With this, it is straightforward to determine the mean estimated parameter for this pattern, along with our confidence for this estimate. We use Bayes Theorem to express this in terms of the prior distributions,

$$\mathcal{P}(p|\bar{\tau}_{\text{obs}}) = \mathcal{P}(\bar{\tau}_{\text{obs}}|p) \frac{\mathcal{P}(p)}{\mathcal{P}(\bar{\tau}_{\text{obs}})}, \quad (14)$$

all of which are readily determined by sampling our committee.

Selecting K parameter values uniformly distributed between the training values, $p^k = p^{(0)}, p^{(0)} + \Delta p, p^{(0)} + 2\Delta p, \dots, p^{(1)}$, we generate N samples at each of these parameter values. The samples are presented to the committee of networks and thus for each sample \mathbf{X}_i drawn at each parameter value p^k , its average truth value $\bar{\tau}_i^k$ is computed. The $\bar{\tau}$'s will take on discrete values, $\bar{\tau} = 0, 1/N_{\text{net}}, 2/N_{\text{net}}, \dots, 1$, and we let n_j^k be the number of samples drawn at p^k with $\bar{\tau}_i^k = j/N_{\text{net}}$. Since we have the same number of patterns in each of the K sample sets, the prior for the parameter is essentially uniform: $\mathcal{P}(p) = \sum_k \delta(p - p^k)/K$. The probability of getting any of the possible discrete values of $\bar{\tau}$ is proportional to the total number of times it occurs for all the samples: $\mathcal{P}(\bar{\tau}_j) = \frac{1}{KN} \sum_k n_j^k$. And finally, given the true input parameter value is p^k , the probability of the committee generating the average truth value $\bar{\tau}_j$ is given by $\mathcal{P}(\bar{\tau}_j|p^k) = n_j^k/N$. Taken together, we have the posterior probability distribution

$$\mathcal{P}(p|\bar{\tau}_j) = \frac{\sum_k \delta(p - p^k) n_j^k}{\sum_{k'} n_j^{k'}}. \quad (15)$$

For our observed pattern, we have the parameter estimate

$$p_{\text{obs}} = \frac{\sum_k p^k n_j^k}{\sum_k n_j^k}, \quad (16)$$

i.e., the parameter-weighted mean. We also get the 68% confidence width for our estimate without any extra work:

$$\sigma^2(p_{\text{obs}}) = \frac{\sum_k (p^k)^2 n_{\text{obs}}^k}{\sum_k n_{\text{obs}}^k} - (p_{\text{obs}})^2 \quad (17)$$

Having the probability distribution Eqn 15 allows us to determine explicit upper and lower confidence intervals, along with the standard error of our parameter estimate.

So far we have outlined how to make a single pass through our parameter estimation method. We must also determine when we have converged on the best estimate. There are three ways the

results generated by the above algorithm can be sub-optimal: i) the true parameter is either too close to either end of the training range $[p^{(0)}, p^{(1)}]$ or outside it; ii) the training range is too broad; or iii) the training range is too narrow. The distributions used to determine Eqn 15 also allow us to test for each of these cases. If the first case did occur, then we have $|p^{(i)} - p_{\text{obs}}| < \sigma(p_{\text{obs}})$ for either $i = 0$ or $i = 1$. Assuming this is not the case, if $\sigma(p_{\text{obs}})$ is much smaller than $p^{(1)} - p^{(0)}$, then we have too broad a training range. We should chose a new training range centered around the current estimate p_{obs} and a width comparable to $\sigma(p_{\text{obs}})$. A too narrow training range is indicated by $\sigma(p_{\text{obs}}) \sim p^{(1)} - p^{(0)}$ and a new broader range needs to be used.

We find it beneficial to supplement the above tests by presenting the committee of trained networks with an independent set of sample patterns drawn at the estimated parameter. The distribution of estimated parameters for this set should not peak near either end of the training range and have a width comparable to the training range. The range is too narrow if the distribution does not have a well-defined shape; is flat around the range. In practice convergence typically requires only two or three iterations.

3. Application: Cosmic Microwave Background Maps

To illustrate this algorithm, we fit the spectral index for CMB anisotropies based on a Gaussian model, an example of the type of problem that will need accurate methods with low computational cost. Deriving cosmological parameters from maps of the cosmic microwave background usually involves maximum likelihood algorithm whose computational cost (N^3) makes them prohibitive for mega-pixel maps. Our neural network method provides rapid parameter estimation for CMB maps.

On angular scales $\theta > 2^\circ$, anisotropy in the cosmic microwave background corresponds to primordial density perturbations with scale-free power spectrum $P_k \propto k^n$, where k is the wavenumber and n is the power-law index. This comes about as quantum fluctuations of the metric during inflation are pushed outside the causal horizon, becoming classical in the process. Later, after inflation has ended, the causal horizon catches up to the fluctuations and they reenter.

We expand full-sky anisotropy maps in terms of spherical harmonics:

$$\frac{\Delta T}{T}(\theta, \phi) = \sum_{l,m} a_{lm} Y_{lm}(\theta, \phi). \quad (18)$$

Since the primordial fluctuations are assumed to have amplitudes that are independent Gaussian processes for each wavenumber, maps are readily generated by projecting these processes onto the expansion coefficients a_{lm} . This amounts to letting the a_{lm} 's be random Gaussian variables with zero mean and the variance (Bond and Efstathiou 1987)

$$\langle |a_{lm}|^2 \rangle = \left(\frac{5Q^2}{4\pi} \right) \frac{\Gamma(l + (n - 1)/2)\Gamma((9 - n)/2)}{\Gamma(l + (5 - n)/2)\Gamma((3 + n)/2)}. \quad (19)$$

Our maps are parameterized by the spectral index n and the amplitude Q . We now see clearly why our maps are stochastic patterns: it is only the statistical properties that are specified by our model. Moreover, these properties are not local for it is in the harmonic conjugate space of our maps that we draw independent random variables. Our networks will learn these non-local statistical correlations as they are trained on different realizations from the above parameterized distributions.

3.1. Instrument modeling

To be able to estimate the parameters for observed data sets, we need to include instrument effects to the pure theory sky maps we generate. The first effect is the pixelization of the full sky. We use the pixelization scheme used by the *COBE*-DMR data, which results in a total of 6144 pixels, each of size $2.5^\circ \times 2.5^\circ$. To generate a single realization, to each a_{lm} , up at an $l_{max} = 20$, we assign a Gaussian random number with width given by Eqn. 19 and evaluate Eqn. 18 with the angular coordinates centered on each pixel: $(\theta, \phi) \rightarrow (\theta_i, \phi_i)$, $i = 1, \dots, 6144$. This pixel resolution oversamples the resolution of the radiometer horn. To account for the radiometer horn profile, we smooth each of these full-sky maps with a Gaussian profile with a FWHM of 7° .

As true for all measurements, the detectors introduce noise into the signal. The scanning strategy for COBE was to visit each pixel many times. Each visit is accompanied by the introduction of Gaussian noise to the signal. Since each addition of noise to each pixel is an independent random process, the more often a pixel is visited, the more the noise is suppressed. We model this by adding Gaussian noise to each pixel with the variance $(20 \text{ mK})^2/N_{\text{obs},i}$, where $N_{\text{obs},i}$ is the number of observations of pixel i (Bennett *et. al.* 1996). (In truth, the pixels are visited in pairs and differences measured; the analysis of the above reference takes this into account.)

Foreground emission from our Galaxy dominates the COBE data near the Galactic plane, rendering it unusable for cosmological analyses. We use the galaxy cut template of (Banday *et. al.* 1997) to excise pixels with significant Galactic emission. The cut sky represents an additional challenge for standard maximum-likelihood analyses. In the absence of this cut, the data sets represent full-sky coverage and can be decomposed in terms of orthogonal spherical harmonics. The resulting coefficients yield the power spectrum of the CMB and hence the spectral index n . Once the galaxy cut is imposed, the spherical harmonic functions are no longer orthogonal on the remaining pixels. Any attempt to obtain a harmonic expansion will result in the aliasing of power between modes and an inaccurate power spectrum. Though a new orthogonal set of basis functions can be computed for the cut sky (Górski, 1994), this is an N^3 problem as well. Since neural networks estimate cosmological parameters using the real-space pixel values, they need not take the detour through the power spectrum, and do not suffer aliasing of power. We simply impose the cut for galactic emission and train each network using only the remaining high-latitude pixels. As the network is trained, it automatically learns the effect of cuts in the data, without requiring any symmetries in the cut data (see *e.g.* Oh *et. al.* 1999).

The final step in processing our raw theory maps is to fit and remove the dipole and quadrupole moments. Our peculiar motion, due to the our motion in the galaxy and the galaxy’s motion through the universe, gives rise to a non-cosmological dipole in the observed CMB anisotropy. The quadrupole is removed because it is dominated by local galactic emission and at the same time contains very little cosmological information.

3.2. Training, sampling and results

We generate simulated COBE maps for fixed $Q = 20\mu K$ and use the spectral index n as the parameter to estimate. Working at the COBE-DMR resolution and after the galaxy cut, this leaves an input pattern of $N_d = 3881$ pixels. We use $N_{\text{Hidden}} = 600$ and $N_{\text{Train}} = 12000$, along with the learning rate $\eta = 0.0188$ and initialize the weights with a zero mean Gaussian of width 0.35 (determined to be the optimal choices). We globally rescale the input patterns so the variance for *all* patterns in both training sets is unity. We can not do this per training set since the variance of a sky map is dependent on the spectral index n . We train 50 networks over the parameter range $n^{(0)} = 0.0$ and $n^{(1)} = 2.0$. To build the probability distribution Eqn 15, we use $K = 17$ parameter values ranging from $n^{(0)}$ and $n^{(1)}$, with $N = 1000$ sample patterns per sample set. Figure 3 plots the probability distribution of n_{obs} for a set of 1000 samples of $n_{\text{in}} = 1.40$ (dotted line). This distribution matches with separation of the training sets and we need this only training iteration. We recover $\bar{n}_{\text{obs}} = 1.30$, with 68% of the samples between 1.07 and 1.51. In terms of our Bayesian analysis, for $n \sim 1$, we determine $\sigma = 0.35$, in agreement with the traditional maximum likelihood analysis of the COBE-DMR 2 year data (Górski *et. al.* 1994).

Note that the neural network algorithm recovered the correct spectral index even though none of the networks used were trained at this value. The uncertainty, derived from the width of the probability distribution of n_{obs} , is comparable to the value predicted by the maximum likelihood method. Neural networks can recover cosmological parameters from CMB data sets with comparable precision as maximum likelihood techniques, but using $N^{1.5}$ calculations instead of N^3 .

4. Scaling of Computational Cost

Neural nets have many desirable characteristics for parameter estimation with mega-pixel CMB maps. They operate globally on the data and return unbiased estimates of the underlying parameter values. They automatically account for data gaps, instrument noise, and other features peculiar to a particular data set. Most importantly, the computational costs are low enough to allow extension to the mega-pixel data sets expected in the near future.

The dominant contribution to the CPU cost is the array multiplication associated with the weights. This multiplication is performed twice per training pass: once for evaluating the pattern, then again for back propagating the error. Each operation scales as the number of weights. Our

total computational cost for training a network is

$$N_{\text{CPU}} = 2N_{\text{Train}}(N_{\text{Hidden}}(N_d + 2) + 1) \quad (20)$$

How this cost scales with N_d depends on the problem being considered.

We derive the scaling for CMB maps by analyzing the CPU costs as progressively larger and larger areas of the sky are covered. In this way, new information is introduced into the data sets as the patch size increases. The S/N ratio per pixel is fixed in this scheme, reflecting the trend in current experiments of scanning ever larger portions of the sky at (roughly) constant S/N ratio per pixel.

We select circular patches of sky centered at the north zenith. The range of patch sizes are chosen to cover 1.5 orders of magnitude in N_d . The number of training passes and the number of hidden units depends on the number of input pixels, *i.e.*, the patch size. For each patch size, we determine which N_{Hidden} gives the best N_{CPU} for a fixed training accuracy. For a range of N_{Hidden} , we train multiple networks on large sets of patterns, also varying the learning rate and width of the Gaussian used to initialize the weights. As the networks are being trained, we monitor their ability to correctly classify independent samples via f_C introduced earlier. Once this ability passes a pre-set threshold, we know N_{Train} for each network, and hence N_{CPU} . We repeat for multiple networks to estimate the uncertainty in the CPU cost. For any fixed patch size, we find the optimal learning rate strongly depends on N_{Hidden} , while the results for N_{CPU} are not strongly dependent on the precise value of N_{Hidden} . Above a minimum value, as N_{Hidden} increases, the number of training passes needed decreases in such a way that N_{CPU} remains constant over a wide range of N_{Hidden} . The results are shown in Figure 4. The computational cost for training a CMB network scales according to $N_{\text{CPU}} \sim N_d^{1.5}$, a considerable improvement over the N_d^3 scaling behavior for a maximum likelihood analysis.

5. Discussion

We have shown neural networks can be used as a tool for astrophysical parameter estimation. For specificity, we have worked in the cosmological context of CMB anisotropy maps where the stochastic nature of the problem is fundamental. The results are insensitive to noise levels and sampling schemes typical of large astrophysical data sets and provide parameter estimation comparable to maximum likelihood techniques.

If we classify parameter estimation techniques as to whether they are forward or reverse algorithms, we see the real strength of neural networks. Maximum-likelihood methods are an example of reverse algorithms. They start with the statistic under consideration and work backwards, inverting a covariance matrix, to the likelihood function used to compare different parameter choices. Forward algorithms provide a way to avoid the high computational costs of inverse methods. Typically, it is much simpler to generate model predictions at each sampled point in parameter space than to

compute the matrix inverse and determinant required for maximum likelihood techniques. Forward algorithms trade many realizations of synthetic data sets computed at specific parameter values for the computationally infeasible matrix inversion. Neural networks are such an algorithm; synthetic data sets are used to both train and sample the networks. This gives us our speed improvement.

Since either maximum likelihood or neural networks can be viewed as the “machinery” for parameter estimation, the fundamental information flow stays the same (see Figure 1). The statistical confidence levels for the fitted parameters are always accessible. When the “machinery” is sampled with independent synthetic data, we can determine the probabilities for making correct or incorrect parameter identifications. Such sampling also gives us direct access to the statistical power (Phillips & Kogut 2001). While training, the information distinguishing the different parameters is encoded in the weights. Interpreting the resulting weight matrices is not usually possible (as compared to the Fisher matrix, Eqn 11). Using independent sampling of the network to derive the probability distributions needed for, *e.g.* Bayesian analysis, means we do not need direct access to the information in the weight matrices.

Neural networks do not require that we specify one single statistic of *a priori* interest, a limitation of maximum likelihood. As the network is trained, it determines how it will discriminate. The information required to separate different parameter points comes from the training set simulations. This lack of a need for a goodness-of-fit function can make neural networks ideal for questions that have been traditionally hard to answer. These include probing the global topology of the universe (Lachièze-Rey & Luminet 1995; Levin *et. al.* 1998) and exploring the viability of non-Gaussian models of structure formation. Both of these problems involve detecting global features in the data sets and there is no strong consensus as to the best statistic to use. The often used power spectrum fails to capture enough information to decisively test either hypothesis. If there is a non-trivial topology to the universe, then the isotropy of the universe assumed when using the power spectrum is broken. Neural networks may turn out to be the ideal method for detecting the global features that would be present if indeed the universe does have a non-trivial topology. Any non-Gaussianity present in the primordial fluctuations that seed structure formation is beyond the power spectrum’s ability to identify, since it measures the second moment. The bispectrum (Heavens 1998; Ferreira *et. al.* 1998; Phillips & Kogut 2001) (the harmonic conjugate of the three point correlation function) is often used to detect evidence of a departure from pure Gaussian. Neural networks, when combined with a non-Gaussian theory, will provide a complement to bispectrum tests.

Along with the explicit example we have presented here of Cosmic Microwave Background anisotropy data, neural networks as a tool for parameter estimation has application to other types of data. Redshift surveys such as the 2-Degree Field and the Sloan Digital Sky Survey measure the redshift and position on the sky of a large number of galaxies ($N \sim 10^6$), sampling the quasi-linear regime $\sim 100h^{-1}$ Mpc where h is the Hubble constant in units $100 \text{ km s}^{-1} \text{ Mpc}^{-1}$. The observed redshift is the sum of the Hubble flow and the peculiar velocity induced by gravitational acceleration in the evolving density field. Coherent flows on large scales produce artifacts in the

redshift distribution compared to real space. Galaxies on the far side of an overdensity tend to flow toward the center (hence toward the observer) so that their peculiar velocities subtract from the Hubble flow, making them appear closer than they really are. Galaxies on the near side move the opposite direction, so their peculiar velocities add to the Hubble flow. The net result is an apparent enhancement in the galaxy density in redshift space on scales of superclusters, compressing the region along the line of sight to the observer. The amplitude of this “bull’s-eye” effect depends on the matter density Ω_m on scales comparable to superclusters of galaxies and can be used to determine Ω_m in model-independent fashion (Praton *et. al.* 1997; Melott *et. al.* 1998).

Estimating Ω_m from distortions in redshift space has several problems in practice. The first is defining a statistic to quantify the bull’s-eye enhancement in concentric rings about the origin. (Melott *et. al.* 1998) use a large number of simulations to develop an empirical statistic defined as the ratio of rms spacing between upcrossings in isodensity contours in the redshift (radial) direction to that in the orthogonal (azimuthal) direction. It is thus a local statistic in that it compares high-density regions only to other nearby regions, and operates only on a single slice of redshift space after smoothing and contouring.

Neural nets, by contrast, offer a *global* test by comparing each region of the density field to all other regions simultaneously, and can easily be extended across the entire three-dimensional survey. No *a priori* statistic need be identified, nor do neural nets require contouring of the density field, thus avoiding the need to “fine-tune” the selection of contour levels.

Neural networks offer a promising approach to cosmological parameter estimation, where the statistical properties of the primordial matter and energy distribution provide one of the few falsifiable tests of the standard inflationary paradigm. They do this at a computational cost much lower than traditional maximum likelihood methods. In the context of CMB anisotropy maps, this cost, $O(N_d^{1.5})$, is better or comparable to the best approximate methods.

REFERENCES

- Andreon, S., Gargiulo, G., Longo, G., Tagliaferri, R. & Capuano, N. (2000). Wide field imaging - I. Applications of neural networks to object detection and star/galaxy classification. *Monthly Notices of the Royal Astronomical Society*, **319**, 700–716.
- Bailer-Jones, C. A. L., Irwin, M., Gilmore, G. & von Tittel, T. (1997). Physical parametrization of stellar spectra - The neural network approach. *Monthly Notices of the Royal Astronomical Society*, **292**, 157 - 166.
- Bailer-Jones, C. A. L., Irwin, M. & von Tittel, T. (1998). Automated classification of stellar spectra - II. Two-dimensional classification with neural networks and principal components analysis. *Monthly Notices of the Royal Astronomical Society*, **298**, 361 - 377.
- Bailer-Jones, C. A. L. (2000). Stellar parameters from very low resolution spectra and medium

- band filters. T_{eff} , $\log g$ and $[M/H]$ using neural networks. *Astronomy and Astrophysics*, **357**, 197 - 205.
- Banday, A.J., Górski, K.M., Bennett, C.L., Hinshaw, G., Kogut, A., Lineweaver, C., Smoot, G.F., & Tenorio, L. (1997). Root Mean Square Anisotropy in the COBE DMR Four-Year Sky Maps. *Astrophysical Journal*, **475**, 393 - 398.
- Bennett, C. L., Hinshaw, G., Jarosik, N., Mather, J. C., Meyer, S. S., Page, L., Skillman, D., Spergel, D. N., Wilkinson, D. T. & Wright, E. L. (1995). The Microwave Anisotropy Probe (MAP) Mission Concept. *187th American Astronomical Society Meeting*, #71.09.
- Bennett, C. L., Banday, A. J., Gorski, K. M., Hinshaw, G., Jackson, P., Keegstra, P., Kogut, A., Smoot, G. F., Wilkinson, D. T., & Wright, E. L. (1996). Four-Year COBE DMR Cosmic Microwave Background Observations: Maps and Basic Results. *Astrophysical Journal*, **464**, L1 - L4.
- Bishop, C. (1995). *Neural Network for Pattern Recognition*, Oxford: Oxford University Press.
- Bond, J. R., & Efstathiou, G. (1987). The statistics of cosmic background radiation fluctuations. *Monthly Notices of the Royal Astronomical Society*, **226**, 655-687.
- Bond, J. R., Efstathiou, G., & Tegmark, M. (1997). Forecasting cosmic parameter errors from microwave background anisotropy experiments. *Monthly Notices of the Royal Astronomical Society*, **291**, L33-L41.
- Bond, Jaffe, & Knox 1998 (1998). Estimating the power spectrum of the cosmic microwave background. *Physical Review D*, **57**, 2117–2137.
- Borrill, J. (1999). Power spectrum estimators for large CMB datasets. *Physical Review D*, **59**, 027302.
- Bunn, E. F. & Sugiyama, N (1995). Cosmological Constant Cold Dark Matter Models and the COBE Two-Year Sky Maps. *Astrophysical Journal*, **446**, 49-53.
- Christensen, N. & Meyer, R. (2000). Bayesian Methods for Cosmological Parameter Estimation from Cosmic Microwave Background Measurements. Los Alamos preprint <http://arXiv.org/abs/astro-ph/0006401>.
- Davis, L. S. (1975). A survey of edge detection techniques. *Computer Graphics and Image Processing*, **4**, 248–270.
- Doré, O., Knox, L & Peel, A. (2001). CMB power spectrum estimation via hierarchical decomposition. *Physical Review D*, **64**, 083001.
- Ferreira, P. G., Magueijo, J. & , Górski, K. M. (1998). Evidence for Non-Gaussianity in the COBE DMR 4 Year Sky Maps. *Astrophysical Journal Letters*, **503**, L1-L4.

- Górski, K. M., Hinshaw, G., Banday, A. J., Bennett, C. L., Wright, E. L., Kogut, A., Smoot, G. F. & Lubin, P. (1994). On determining the spectrum of primordial inhomogeneity from the COBE DMR sky maps: Results of two-year data analysis. *Astrophysical Journal*, **430**, L89–L92.
- Górski, K. M., Banday, A. J., Bennett, C. L., Hinshaw, G., Kogut, A., Smoot, G. F. & Wright, E. L. (1996). Power Spectrum of Primordial Inhomogeneity Determined from the Four-Year COBE DMR Sky Maps. *Astrophysical Journal*, **464**, L11–L15.
- Gott, J. R. I., Park, C., Juszkiewicz, R., Bies, W. E., Bennett, D. P., Bouchet, F. R. & Stebbins, A. (1990). Topology of microwave background fluctuations - Theory. *Astrophysical Journal*, **352**, 1–14.
- Heavens, A. F. (1998). Estimating non-Gaussianity in the microwave background. *Monthly Notices of the Royal Astronomical Society*, **299**, 805–808.
- E. Hivon, E., Górski, K. M., Netterfield, C.B., Crill, B.P., Prunet, S. & Hansen, F. (2001). MASTER of the CMB Anisotropy Power Spectrum: A Fast Method for Statistical Analysis of Large and Complex CMB Data Sets. Los Alamos preprint <http://arXiv.org/abs/astro-ph/0105302>.
- Hough, P.V.C., (1962). *Method and Means for Recognizing Complex Patterns*, US Patent 3,069,654
- Kogut, A., Banday, A. J., Bennett, C. L., Górski, K. M., Hinshaw, G., Smoot, G. F. & Wright, E. L. (1996). Tests for Non-Gaussian Statistics in the DMR Four-Year Sky Maps. *Astrophysical Journal*, **464**, L29–L33.
- Kendall, M. G. & Stuart, A. (1966). The advanced theory of statistics, Volume 3: Design and analysis, and time-series. New York: Hafner Pub. Co.
- Lachièze-Rey, M & Luminet, J-P (1995). Cosmic topology. *Physics Reports*, **254**, 135–214.
- Lahav, O., Naim, A., Sodr ´, L., Jr. & Storrie-Lombardi, M. C. (1996). Neural computation as a tool for galaxy classification: methods and examples. *Monthly Notices of the Royal Astronomical Society*, **283**, 207–221.
- Levin, J., Scannapieco, E. & Silk, J. (1998). The topology of the universe: the biggest manifold of them all. *Classical and Quantum Gravity* **15** 2689–2697.
- MacKay, D. J. C. (1995). Probable networks and plausible predictions—a review of practical Bayesian methods for supervised neural networks. *Network: Computation in Neural Systems*, **6** 469–505.
- Melott, A. L., Coles, P., Feldman, H., & Wilhite, B. (1998). The Bull’s-Eye Effect as a Probe of Omega. *Astrophysical Journal Letters*, **496**, L85–L88.

- Oh, S.P., Spergel, D.N., & Hinshaw, G. (1999). An Efficient Technique to Determine the Power Spectrum from Cosmic Microwave Background Sky Maps. *Astrophysical Journal*, **510**, 551–563.
- Phillips, N.G., & Kogut, A. (2001). Statistical Power, the Bispectrum, and the Search for Non-Gaussianity in the Cosmic Microwave Background Anisotropy. *Astrophysical Journal*, **548**, 540–549.
- Praton, E. A., Melott, A. L., & McKee, M. Q. (1997). The Bull’s-Eye Effect: Are Galaxy Walls Observationally Enhanced? *Astrophysical Journal*, **479**, L15–L18.
- Rocha, G., Magueijo, J., Hobson M. & Lasenby, A. (2001). Bayesian joint estimation of non-Gaussianity and the power spectrum. *Physical Review D*, **64**, 063512.
- Tagliaferri, R., Ciaramella, A., Milano, L., Barone, F. & Longo, G. (1999). Spectral analysis of stellar light curves by means of neural networks. *Astronomy and Astrophysics Supplement*, **137**, 391–405.
- Tegmark, M., Taylor, A. N., & Heavens, A. F. (1997). Karhunen-Loeve Eigenvalue Problems in Cosmology: How Should We Tackle Large Data Sets? *Astrophysical Journal*, **480**, 22–35.
- Vogeley, M. S. & Szalay, A. S. (1996). Eigenmode Analysis of Galaxy Redshift Surveys. I. Theory and Methods. *Astrophysical Journal*, **465**, 34–53.

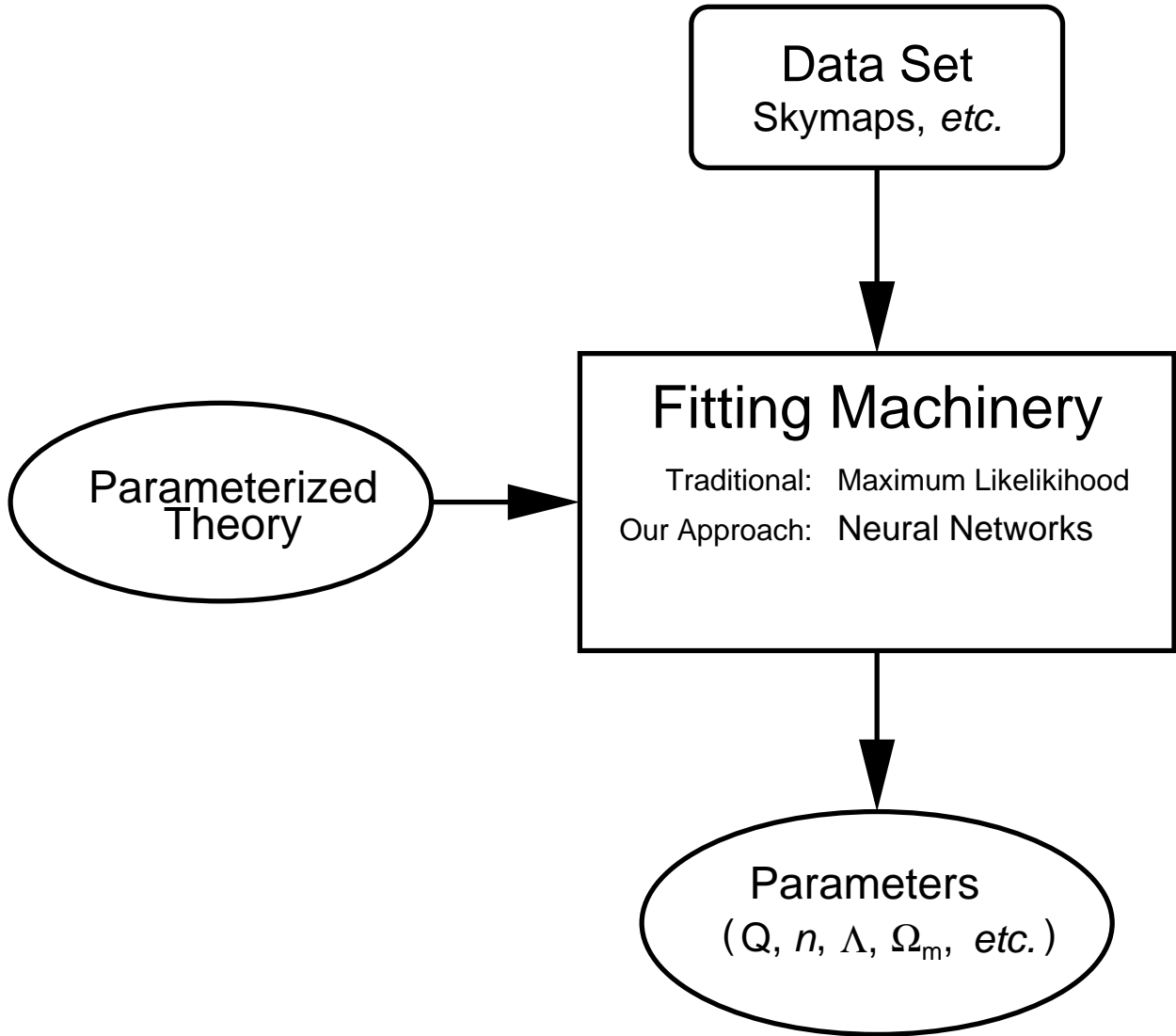


Fig. 1.— Our basic model for parameter estimation from a data set. We have to *a priori* assume a model to compare the observed data set against; what we pay attention to is the machinery for performing this comparison. Maximum likelihood methods, the *de facto* standard in the CMB community must assume a model, just as must be done with currently proposed neural network method.

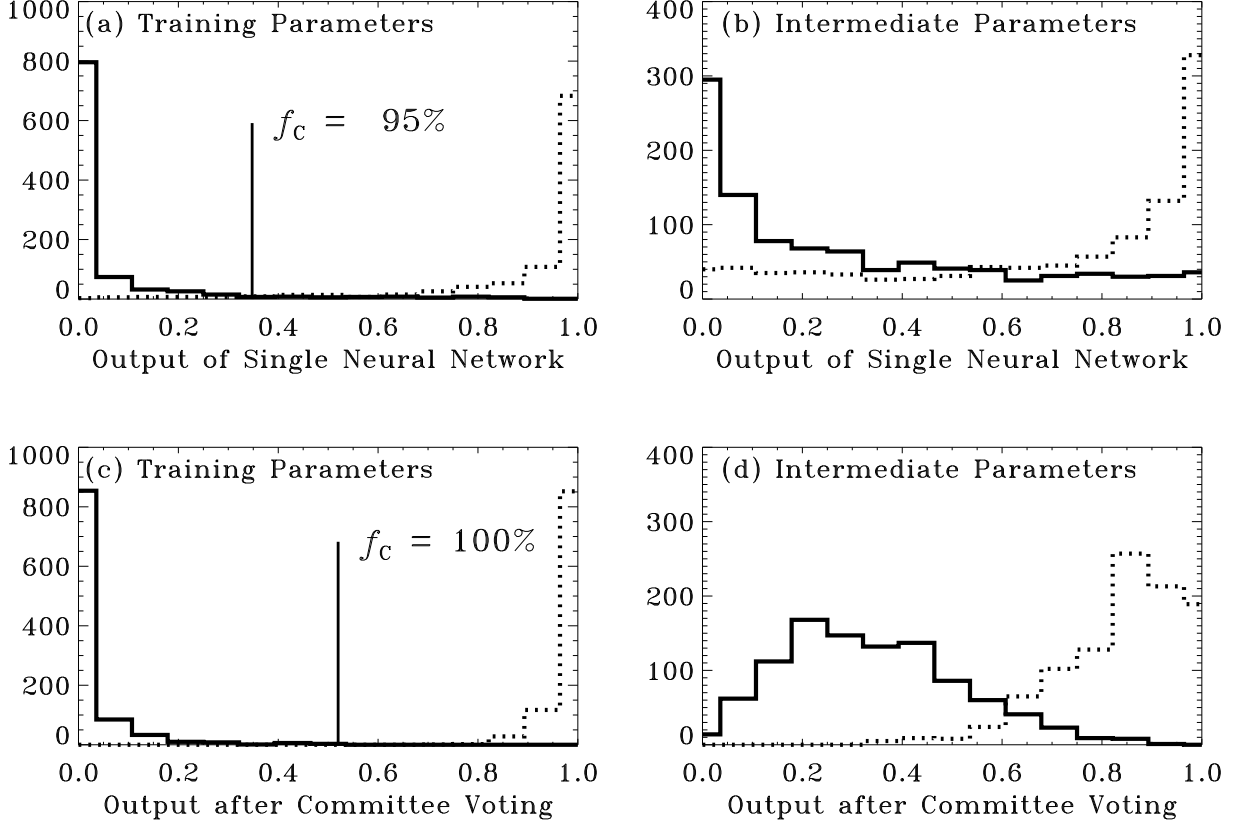


Fig. 2.— Sample neural network output distributions. (a) Solid line is the distribution of output values for an independent set of samples drawn at the same parameter value $p^{(0)}$ for which the network was trained to the target 0. The dotted line is for samples drawn at $p^{(1)}$, the value for the target 1. The vertical line is the midpoint value o_{mid} that maximizes the fraction correct f_C , *i.e.*, all output values $< o_{\text{mid}}$ are identified as being drawn at $p^{(0)}$ while the rest at $p^{(1)}$. (b) The output of the same network, but for samples drawn at parameters intermediate to $p^{(0)}$ and $p^{(1)}$. The solid line is for p close to $p^{(0)}$ and the dotted line for a choice close to $p^{(1)}$. (c) Solid line is the average truth value \bar{t} for the $p^{(0)}$ patterns, averaged over a committee of 50 networks, the only difference between the networks being the initial randomization of the weights. The dotted line is for $p^{(1)}$. (d) The average truth value for the same sets of samples in (b). The averaging has produced two well defined peaks that are cleanly separated. Distributions of \bar{t} like those in (c) and (d) become the basis for predicting which estimated parameters to associate with the average truth values, the output due to presenting a committee of networks with an unknown pattern.

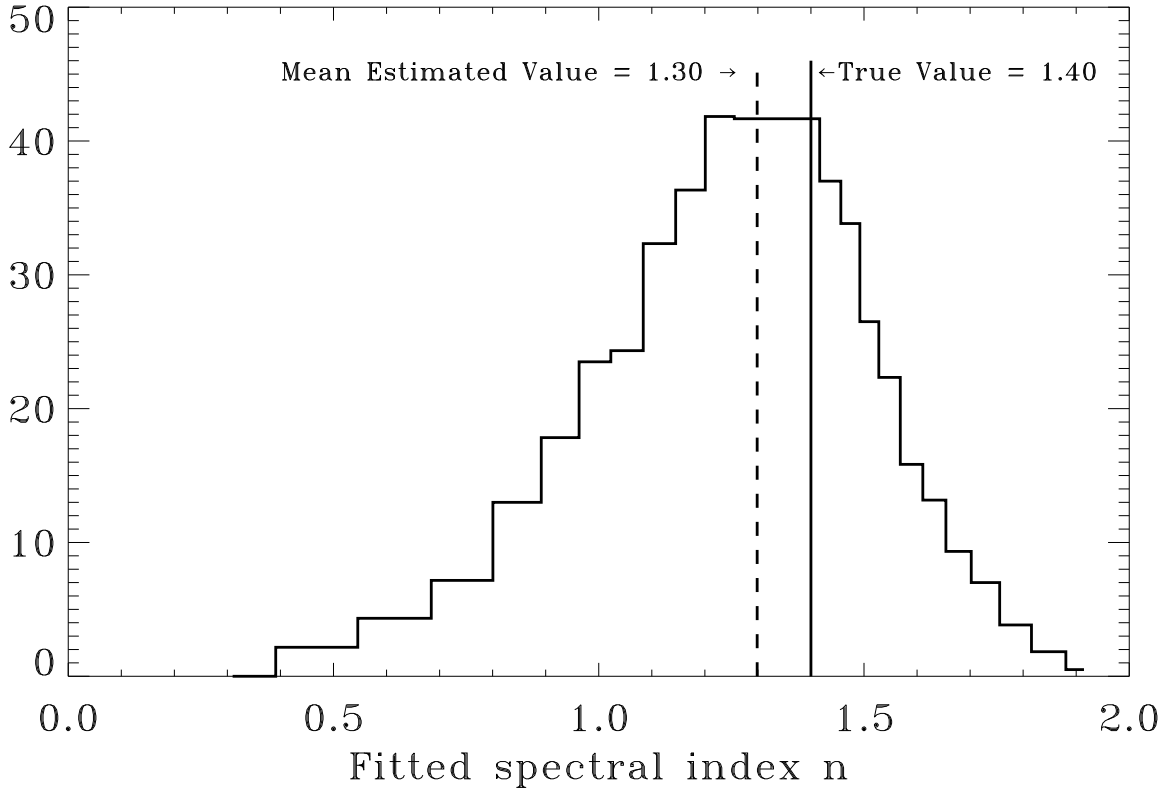


Fig. 3.— Fitted spectral index n_{obs} derived from 1000 realizations of CMB anisotropy sky maps with $n_{\text{in}} = 1.25$. The dotted line is for an initial training range of $n^{(0)} = 0.5$ and $n^{(1)} = 1.5$ while the solid line is the distribution for the final range of $n^{(0)} = 0.8$ and $n^{(1)} = 1.4$. The fitted values correctly peak at the input value (vertical solid line), despite never having trained on this parameter value.

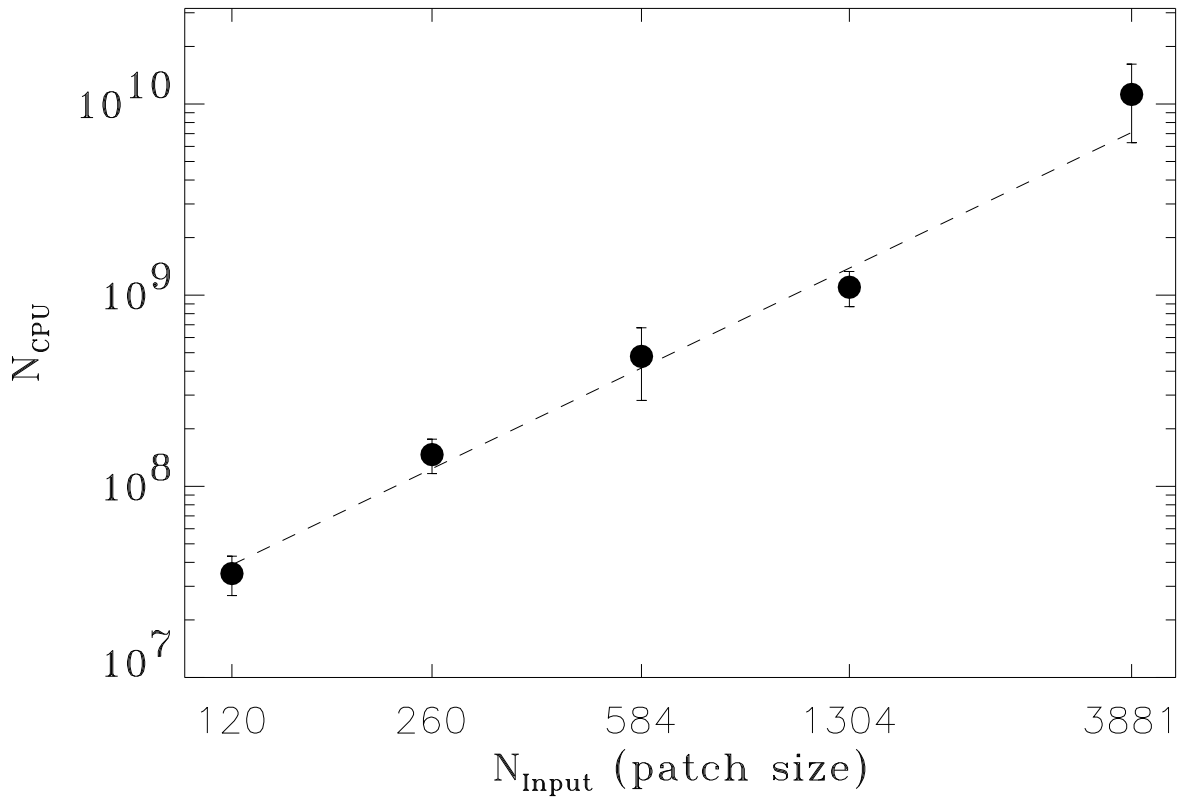


Fig. 4.— Scaling of computational costs for CMB anisotropy. Working at a fixed sky map resolution, we vary the patch size that is examined. This holds the S/N per pixel fixed, but new information is introduced as the patch size increases. The solid line represents a power law fit of $N_{\text{CPU}} \sim N_d^{1.5}$.